Coarse-grained and All-atom Simulations towards the Early and Late Steps of Amyloid Fibril Formation

Article *in* Israel Journal of Chemistry (Online) · August 2016

DOI: 10.1002/ijch.201600048

6 authors, including:

Mara Chiricotto
Institute of Physical and Chemical Biology
5 PUBLICATIONS **16** CITATIONS

SEE PROFILE

Simone Melchionna
Italian National Research Council
142 PUBLICATIONS **2,562** CITATIONS

SEE PROFILE

Fabio Sterpone
French National Centre for Scientific Resea…
56 PUBLICATIONS **1,139** CITATIONS

SEE PROFILE

Philippe Derreumaux
French National Centre for Scientific Resea…
193 PUBLICATIONS **4,134** CITATIONS

SEE PROFILE

Review

Israel Journal of Chemistry

DOI: 10.1002/ijch.201600048

Coarse-grained and All-atom Simulations towards the Early and Late Steps of Amyloid Fibril Formation

Mara Chiricotto[†],[a] Thanh Thuy Tran[†],[a] Phuong H. Nguyen,[a] Simone Melchionna,[b] Fabio Sterpone,[a] and Philippe Derreumaux*[a]

Abstract: Alzheimer's disease is the most common neurodegenerative disease. Experiments and computer simulations can complement one another to provide a full and in-depth understanding of many aspects in the amyloid field at the atomistic level. Here, we review results of our coarse-grained and all-atom simulations in aqueous solution aimed at determining: 1) early aggregation steps of short linear peptides; 2) nucleation size number; 3) solution structure of the $A\beta_{1-40}/A\beta_{1-42}$ wild-type dimers; 4) impact of FAD (familial forms of Alzheimer's disease) mutations on the structure of $A\beta_{1-40}/A\beta_{1-42}$ dimers; and 5) impact of protective mutations on the structure of $A\beta_{1-40}/A\beta_{1-42}$ dimers.

Keywords: Alzheimer's disease · amyloid simulations · computational chemistry · mutations · oligomerization

1 Introduction

Alzheimer's disease (AD) is the most common neurodegenerative disease and is pathologically characterized by neurofibrillary tangles resulting from the accumulation of hyper-phosphorylated tau protein and by amyloid plaques made of the amyloid beta (Aβ) protein that results from cleavage of the transmembrane amyloid precursor protein (APP) by beta-secretase (BACE1) and gamma-secretase.[1] Despite continuous debate, there is strong evidence that an imbalance between production and clearance of $A\beta_{1-40/1-42}$ and related Aβ proteins (either truncated or post-translational modified) plays a key role in initiating AD.[2,3]

Though research aimed at targeting BACE1,[1] modulating the response of the innate immune system,[4] interfering on Apolipoprotein E4 and other components of cholesterol metabolism, and regulating endosomal vesicle recycling is pursued,[5] controlling Aβ self-assembly with inhibitors is considered as one of the most promising solutions to delay the onset or stop the progression of AD.[6] The challenge arises first from the intrinsically disordered structure of the human wild-type (WT) Aβ monomer in aqueous solution. $A\beta_{1-42}$ WT sequence, DAEFRHDSGYEVHHQKLVFFAEDVGSNKGAIIGLMVGGVVIA, has two hydrophobic patches, L17-A21 (CHC) and A30-A42 (C-terminus), and two hydrophilic patches, E22-G29 (loop region) and D1-K16 (N-terminus).[7] The challenge also comes from the lack of high-resolution structures and formation/dissociation rates of the low molecular weight $A\beta_{1-40/1-42}$ oligomers, including dimers, which are believed to be the most critical players in the pathology;[8,9] and for these oligomers, we have at hand low-resolution structural data.[1] Finally, the experimental sigmoidal kinetics of amyloid formation is the result of a linear combination of microscopic reactions involving primary classical and secondary (fragmentation and surface-dependent lateral) nucleation processes, and we know little on the topology and size of the primary nucleus.[10–13] The kinetics is also sensitive to the experimental conditions and the sequences, with mutations enhancing or reducing fibrillogenesis and toxicity.[6,10]

Here, we review the contribution of my group and collaborators to understanding the early and late aggregation steps of amyloids in aqueous solution based on coarse-grained (CG) OPEP and all-atom simulations. We focus on five aspects and compare with other simulation

[a] M. Chiricotto, T. T. Tran, P. H. Nguyen, F. Sterpone, P. Derreumaux
Laboratoire de Biochimie Théorique
UPR 9080 CNRS
Université Paris Diderot
Sorbonne Paris Cité, IBPC
13 Rue Pierre et Marie Curie
75005
Paris
France
(+33) 1 5841 5172
e-mail: philippe.derreumaux@ibpc.fr

[b] S. Melchionna
Istituto Sistemi Complessi
Consiglio Nazionale delle Ricerche
P. le A. Moro 2
00185
Rome
Italy

[†] Both authors contributed equally.

results and experimental data, when possible. Simulations of Aβ and related peptides interacting with inhibitor candidates, such as EGCG, NQTrp, N-methylated peptides, and carbon nanotubes, or aimed at dissociating amyloid fibrils, are described elsewhere.[14–22]

Prior to amyloid results, we recall that the OPEP (optimized potential for efficient protein structure prediction) CG model represents the amino acid by six centers of force. Each side chain is represented by a unique bead, and the backbone uses an atomic resolution with N, HN, Cα, C, and O atoms. Proline is an exception, represented by all its heavy atoms (Figure 1A).[23,24] The implicit solvent OPEP model retains chemical specificity and is free from any biases. This runs in contrast to the Martini CG model that imposes secondary structure constraints,[25] and the CG Caflisch[26] and Shea[27] models that tune the probability of the monomer to form β-strand. The OPEP energy function is expressed as a sum of local, nonbonded, and hydrogen bonding (H-bond) terms, and all analytical terms are given in Refs. [28,29]. Notably, H-bonds

Mara Chiricotto is currently a Ph.D. student under the supervision of Prof. P. Derreumaux and Dr. F. Sterpone at Laboratoire de Biochimie Théorique, IBPC. She received her B.Sc. and M.Sc. in physical and computational chemistry at University of Rome – La Sapienza. Her research interests are the hydrodynamic effects of amyloid aggregation using multiscale simulation methods.

Simone Melchionna is currently a researcher at the Institute for Complex Systems, of the Italian Consiglio Nazionale delle Ricerche. He has a Ph.D. in chemistry from the University of Rome, Sapienza, during which he developed computational techniques for molecular dynamics of biological systems, such as constrained mechanics, enhanced sampling, and isothermal-isobaric dynamical approaches. Then he moved for three years to Cambridge, where he worked on confined fluids, water, and ion channels via density functional and other theoretical approaches. Subsequently, he worked for three years at Harvard on lattice Boltzmann and multiscale simulation methods, with applications to DNA translocation and blood flow in cardiovascular systems. His research focuses on high-performance computing applied to proteins and other biological systems.

Thanh Thuy Tran is currently a Ph.D. student under the supervision of Prof. P. Derreumaux and Dr. P. H. Nguyen at Laboratoire de Biochimie Théorique, IBPC. She obtained her B.Sc. and M.Sc. in theoretical and mathematical physics at Hanoi University of Education, Vietnam, and her diploma in condensed matter physics at the Abdus Salam International Centre for Theoretical Physics (ICTP), Trieste, Italy. Her research interests are coarse-grained lattice models for amyloid aggregation and all-atom simulations.

Fabio Sterpone is currently a CR1 CNRS researcher at IBPC, Paris. He graduated from the University of Paris UPMC (Biophysics) and occupied several postdoc positions later on; he dealt with quantum classical simulations of materials and the effect of solvent on biomolecular structure and dynamics. Presently, he is mainly interested in the study of protein stability and aggregation in extreme environments by applying and developing multiscale simulation methodologies.

Phuong Nguyen is currently a CR1 CNRS researcher at IBPC, Paris. He obtained his Ph.D. from the Physics Department, Bielefeld University, Germany, and did a postdoc at the Chemistry Department, Frankfurt University, Germany. His current research focuses on the development and application of theoretical methods for studying equilibrium and nonequilibrium structure, dynamics, and thermodynamics of single and amyloid proteins.

Philippe Derreumaux is professor at the University Denis Diderot, Sorbonne Paris Cité. His main research contributions involve coarse-grained model developments for many applications, including neurodegenerative diseases.

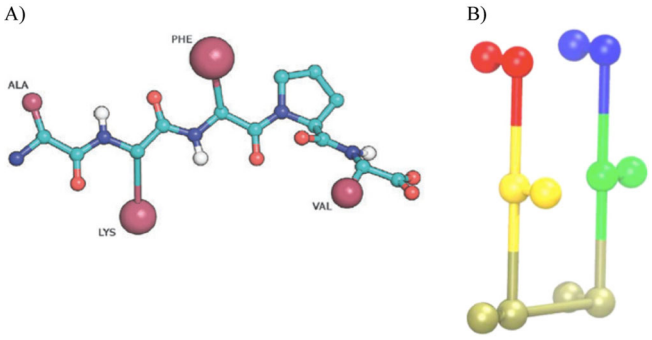

Figure 1. OPEP models. A) The peptide Ala-Lys-Phe-Pro-Val in its zwitterion form shows the details of the backbone and the side chains for the off-lattice model. B) One on-lattice structure of the $A\beta_{37-42}$ peptide Gly^{+}(red)-Gly (yellow)-Val (grey)-Val (grey)-Ile (green)-Ala^{-}(blue). For simplicity, the aliphatic hydrogen of Gly side chain is also shown.

between backbone atoms are modeled by two- and four-body potentials, rather than Coulombic interactions. In contrast to other CG models used for amyloid proteins,[30,31] OPEP has been successfully tested on many non-amyloid proteins, recovering experimental structures and thermodynamic properties,[29,33–37] and protein/protein complexes using various advanced sampling methods.[38]

2 Early Aggregation Steps of Short Linear Peptides

Independently of the sampling method (molecular dynamics (MD), replica exchange molecular dynamics (REMD), and replica exchange Monte Carlo (REMC)), whether CG or all-atom force field with explicit/implicit solvent is used, the self-assembly of short linear peptides starts with the formation of partially ordered oligomers, which is modulated by the hydrophobic character of the system. Then, the formation of H-bonds drives oligomers to transient and marginally populated β-rich aggregates.[39–43]

Using OPEP, we were the first to observe that these β-rich oligomers have various sheet-to-sheet pairing angles,[44] a prediction that was confirmed by X-ray structures of macrocyclic β-sheet mimics[45] and other force field calculations.[28,40] We predicted that these β-rich oligomers can form transient β-barrels,[44,46] and this was validated by the microcrystal structure of an 11-residue amyloid peptide[47] and other simulations,[27,48] and is compatible with IM-MS data.[49] We also identified rare events involving reptation moves of the β-strands,[50,51] allowing the change in the register of the H-bonds without full detachment of the peptides, prior to Fourier transform infrared spectroscopy (FTIR)[52] and atomistic simulation results.[53,54]

Of particular interest from all simulations of 7-mers to 20-mers is that the β-rich oligomers are characterized by a predominance of mixed parallel-antiparallel β-strands, independently of the sequence.[30,39–41,46,55–57] This runs in contrast to the final products, which display either antiparallel or parallel β-strands within the sheets.[58] This β-strand orientation mismatch, also observed experimentally for $A\beta_{1-40/1-42}$ peptides,[1] raises the question about when the transition towards fully parallel or antiparallel intermolecular β-sheets occurs during oligomerization.

Most computer studies of amyloid aggregation have focused on thermodynamics, rather than dynamics, because enhanced advanced sampling from REMD, simulated tempering (ST), and metadynamics does not provide direct information about kinetics. In addition, an accurate description of dynamics obtained from CG models with implicit solvent requires inclusion of computationally demanding hydrodynamic interactions that water exerts on the solute.[59,60] Hydrodynamic interactions arise from the motion of atoms that generate a velocity field in the surrounding aqueous environment and the resulting flow acts on other protein atoms. While hydrodynamic interactions do not impact the equilibrium distribution of states, they affect dynamics and escape from metastable states and have striking effects on the simulated diffusion and folding of proteins.[61]

In this context, we recently presented a novel computational framework that integrates the OPEP CG model for proteins with the lattice Boltzmann molecular dynamics (LBMD) methodology to account for the fluid as a continuum in a probabilistic sense, and determine the explicit and on-the-fly solutions of the fluid dynamics and kinetics.[29] Protein particles are advanced in time by MD, fluid populations are used to represent the solvent and are advanced in time by the lattice Boltzmann equation, and the coupling between the motion of a solute particle and fluid is based on the assumption that momenta exchange in a Stokes fashion, i.e., modeled by a drag force between each particle and the fluid, with one term proportional to the friction coefficient, γ.[62] This parameter is empirically tuned so that the diffusion constant of the molecular system at infinite dilution matches the experimental value.

Figure 2 shows the time evolution of the size of the largest cluster, and the number of free monomers using Langevin dynamics and LBMD simulations of 100 $A\beta_{16-22}$ peptides, starting from 100 randomly placed peptides in a cubic box of size $L = 150$ Å. The aggregation process is characterized by a first timescale (< 10 ns) that controls the first encounter of the peptides and the formation of small oligomers, and a second timescale of 10^2 ns that controls the fusion and the growth of larger aggregates. The first striking effect of the hydrodynamic interactions (HI) is to speed up the early aggregation phase, as highlighted in the inset graphs. The second key effect is that HIs favor the growth of the largest cluster and its size fluctuations. The aggregates behave as active particles, and their change in shape and size alter the surrounding

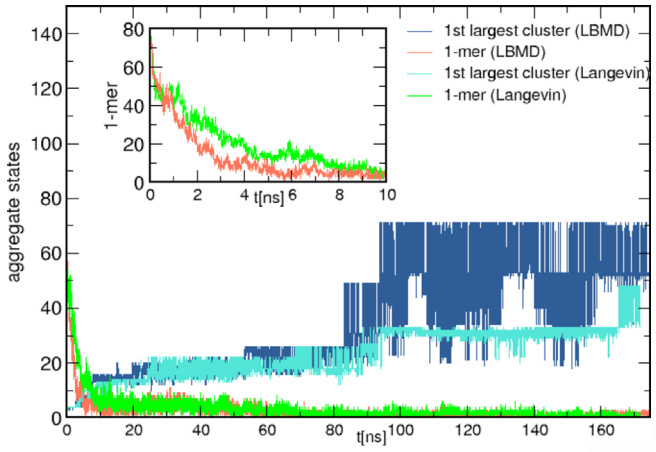

Figure 2. Aggregation results of 100 $A\beta_{16-22}$ peptides. Time evolution of the size of the largest cluster (blue), and the number of free monomers (green and red) in solution, using Langevin dynamics and lattice Boltzmann molecular dynamics (LBMD). The inset shows the monomer population in the first 10 ns. The clusters are defined by considering the distance between the monomer center of mass, and considering a cut-off of 12 Å.

fluid with effect on the inclusions of free monomers in larger clusters, as well as the fusion of separate aggregates. Note that after 300 ns of LBMD (data not shown), all the monomers fuse in a unique elongated 100-mer with 17% β-content, and the simulation time may not correspond to the real aggregation timescale, which is much slower.

In Figure 3, we present the results of an LBMD simulation of a system of unprecedented size composed of 1000 $A\beta_{16-22}$ peptides, placed initially in random positions in a cubic box of size L = 250 Å. Transposed to an explicit solvent all-atom resolution, this system would count 2.4 million particles. A system of such a size allows, when compared with smaller systems, to explore a large number of intermediate states. At the time scale explored in the simulation, 200 ns, we observe a continuous growth of the larger clusters. The jumps observed along the growth curves mirror the sudden absorption of smaller-sized entities. At the end of the simulation, about 30% of the system is assembled in the two larger clusters. Two representative configurations of the largest structures, formed at different times, are also presented. Interestingly, during the growth, we observe the presence of a branched structure with a β-content of 14% (see the snapshot at 200 ns), as predicted by lateral secondary nucleation and observed for some proteins experimentally.

3 Nucleation Size Number

A very important question is that related to the size of the primary nucleus or critical nucleation number, N*. In addition to pH, concentration, and temperature, many

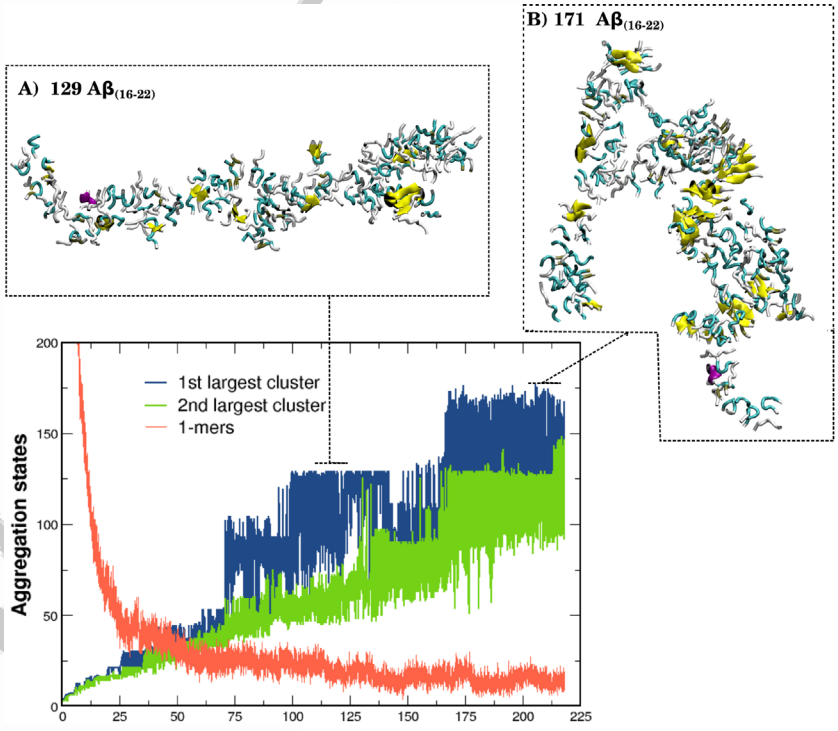

Figure 3. System with 1000 $A\beta_{16-22}$ peptides. Time evolution of the size of the largest cluster (blue), the second largest cluster (green) and the number of free monomers in solution. The panels A) and B) show representative configurations of the largest aggregates explored between 110 and 115 ns and between 210 and 215 ns.

factors are known to modulate N* and the lag-phase time, from experimental studies, as measured by Thioflavin-T Fluorescence,[12,63,64] and theoretical studies, as determined by kinetic models,[65] atomistic nucleation theory,[66] and simulations of mesoscopic and on-lattice models.[11,26,27,67,68] These factors range from salt and metal concentration, energy landscape of the monomer, and population of the monomeric aggregation-prone state, shear flows to the supersaturation of the protein solution. Using simplified models, it has been shown that increasing the total side-chain hydrophobicity switches the fibrilization mechanism from one- to two-step nucleation, where in the one-step nucleation, the β-sheet enriched nucleus forms directly from the solution, and in the two-step nucleation, soluble monomers first assemble into disordered oligomers, which subsequently convert into a β-sheet nucleus.[12,69]

All-atom simulations in explicit solvents were performed to determine N*. By following the stability of preformed β-sheet oligomers by MD or REMD, and characterizing the free-energy landscape from disordered aggregates by REMD or bias-exchange metadynamic simulations, it was suggested that N* varies between 7 to 16 depending on the peptide (e.g., $A\beta_{16-22}$, STVIYE, GVIGIAQ, Val_8).[70–73] Also, the highest free-energy barrier could be associated with the transition from mixed β-strand orientation to native β-strands and the formation of highly interdigitated side chains, the so-called steric zipper.[56,74] The limitation of standard atomistic simulations is that rare events and high-energy states are not properly explored and metadynamic simulation results are very sensitive to the choice of the collective variables.

On-lattice simulations were also conducted to determine N*. Using a hydrophobic-polar energy model, Li *et al.* found that N* = 11 for $A\beta_{1-42}$.[75] By introducing the orientation of the side chains, Irback *et al.* showed that the highest free-energy barriers for an oligomer to form a fibril is accompanied by a change in width.[76] Using specific side-chain interactions, backbone H-bonds and solvent effects, Frenkel *et al.* found that N* = 10 for the amyloid peptide TFTFTFT, with alternating polar and hydrophobic amino acids.[77]

Recently, we went one step beyond, by presenting an OPEP force-field parametrization for the lattice model developed by Frenkel[77] to determine the critical nucleus size of the experimentally well-characterized $A\beta_{16-22}$ and $A\beta_{37-42}$ peptides.[78] A representative structure of $A\beta_{37-42}$ in the lattice representation is shown in Figure 1B. There are various bottom-up approaches to develop coarse-grained potentials matching all-atom simulations or experimental data. Our bottom-up approach starts with the optimization of the lattice force parameters for the $A\beta_{16-22}$ dimer by fitting its equilibrium parallel and antiparallel β-sheet populations to all-atom REMD simulation results, using both CHARMM22*/TIP3P and AMBER-f99SB-ILDN/TIP3P force fields. We found that the OPEP four-body H-bond interaction plays a crucial role in the correct description of secondary structures and end-to-end distributions, and this force field is transferable to the $A\beta_{16-22}$ trimer and the dimers and trimers of $A\beta_{37-42}$, again by comparing with all-atom REMD simulations.[78] Using this set of parameters and extensive REMC simulations at the calculated folding temperature of the monomer, we characterized the free-energy landscapes (FEL) of the 10-mers.

The most populated structures of the $A\beta_{16-22}$ 10-mers, representing more than 90% of the ensemble, display one 10-stranded β-sheet or two 5-stranded β-sheets (Figure 4A), matching the microcrystal and solid-state NMR structures of the amyloid fibril. Experimentally, the $A\beta_{16-}$

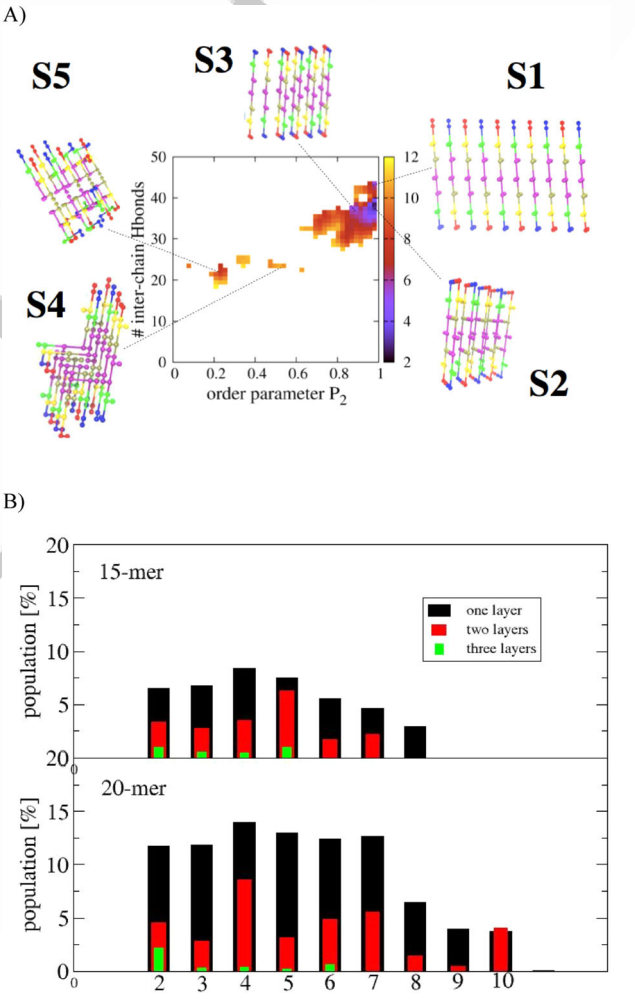

Figure 4. On-lattice OPEP-REMC simulations of $A\beta_{16-22}$ and $A\beta_{37-42}$ peptides. A) The free-energy landscape (in k_BT) of $A\beta_{16-22}$ 10-mers as a function of the order parameter P2 and the total number of intermolecular H-bonds below the melting temperature of the aggregate. Representative structures at the center of all minima are depicted. B) The population of one (black), two (red), and three (green) β-sheet layers as a function of the number of β-strands. Shown are results of the 15-mer (upper) and 20-mer (lower) $A\beta_{37-42}$ below the melting temperature of the aggregates.

$_{22}$ fibril forms antiparallel β-sheets with antiparallel β-strands within individual sheets.[79,80] Additional OPEP-REMC simulations for aggregates between 4- and 12-mers indicate a nucleus size of 10 chains.[78]

The FEL changes completely for the $A\beta_{37-42}$ 10-mers. At room temperature, this oligomer is very disordered and 91% of the conformational ensemble has a total of intermolecular H-bonds ($N_{H\text{-}bond}$) ≤ 12, and an order parameter $P2 \leq 0.3$. This ensemble is characterized by $A\beta_{37-42}$ peptides mainly folded into β-hairpins with turns at residues 39–40, and packed in different architectures. Analysis of the ordered states shows that the experimental fibril state is present with a Boltzmann probability of 2%, indicating that $N^* > 10$ chains.[78] Importantly, in contrast to $A\beta_{16-22}$ fibril, the $A\beta_{37-42}$ amyloid fibril features experimentally parallel β-strands (i.e., with the two end termini identically charged residues in contact) and antiparallel layers of β-sheets.[79]

Because the determination of critical nucleus sizes is important in our understanding of fibril formation mechanisms, we present new OPEP-REMC simulation results of the $A\beta_{37-42}$ peptide for 15-mer and 20-mer, starting from disordered states at the folding temperature of the monomer. Figure 4B shows the population of one, two, and three layers of β-sheets composed of *n*-stranded β-strands. The one-layer architecture is more populated than the two-layer one, and the three-layer structure is hardly formed, and overall, both systems are mainly disordered, as reported by the low population (<15%) of the layers of β-sheets. These results indicate that N^* is >20 chains for $A\beta_{37-42}$.

4 Solution Structure of the $A\beta_{1-40}$/$A\beta_{1-42}$ Wild-type Dimers

The $A\beta_{1-40}$ and $A\beta_{1-42}$ WT dimers in aqueous solution were studied by Hamiltonian replica exchange molecular dynamics coupled to OPEP, all-atom REMD with a solvent-accessible surface-area implicit solvent,[81] discontinuous MD (DMD) with a four-bead CG model,[31] and all-atom MD simulations starting from CG DMD structures.[82] The results of these simulations show many discrepancies in the 3D intra-/inter-molecular structures.[1] To get a better understanding of the equilibrium structures, we studied the $A\beta_{1-40}$ WT dimer by REMD simulations, 400 ns per replica,[83] using the all-atom CHARMM22* force field, considered as one of the best force fields, at least for folded proteins.[84,85] The representative structures of the first 10 overall states of the $A\beta_{1-40}$ WT dimer at 315 K are reported in Ref. [83].

The cross collision sections (CCS) of the first 20 clusters for $A\beta_{1-40}$ WT dimer were found to vary between 1195 and 1322 Å^2, and using all conformations, the averaged CCS value is 1255 Å^2.[83] These values are compatible with two ion mobility-mass spectrometry (IM-MS) studies, based on distinct sample preparations, and leading to a mean CCS of 1142 and 1245 Å^2.[86,87] Note there is experimental evidence that there are multiple structures with different mobilities and cross sections.[87] Using all REMD-generated structures, the percentage of secondary structure averaged over all residues of the $A\beta_{1-40}$ dimer is found to be 18.7±3.3% for β-strand, 10±2.7% for α-helix, 43±3.7% for turn, and 28±3.1% for random coil.[83] This calculated 2D structure is consistent with circular dichroism (CD) analysis, using two sample preparations, which reported α-helix, β-strand, and random coil/turn contents of (10.5, 38.6, and 50.9%) and (0, 12, and 78%).[88,89]

This first all-atom extensive simulation demonstrates the inherently disordered structure of the $A\beta_{1-40}$ WT dimer with high coil/turn content. We observe, however, multiple transient intramolecular β-hairpins spanning the CHC and residues 30–36 that persist from monomer[7,90–94] to dimer simulations, and involve the F19-L34 contact with a lifetime of 34%. The role of this contact on the early oligomers and toxicity has been discussed experimentally.[1,95] Consistent with many models of Aβ oligomers derived from nuclear magnetic resonance (NMR) spectroscopy,[1,96] we find transient antiparallel β-sheets between the two CHCs. Our equilibrium ensemble also reveals: short-lived all-α topologies (Figure 5A); all-β topologies (Figure 5B) with two perpendicular β-sheets; mixed αβ topologies, characterized by one compact peptide, with the β-sheet structure stabilized by a rather extended peptide with α-helical content; and parallel β-sheets between the CHC and the C-terminus, rather than between the two CHCs and between the two C-termini, as observed in the fibrillar states.

Overall, a large structural rearrangement is necessary to fit the fibrillar-like states. We are exploring the $A\beta_{1-40}$ WT dimer with other atomistic force fields by extending each replica to the microsecond time-scale. Indeed it has been shown that there is some dependence of Aβ monomer dynamics and thermodynamics on protein force fields.[94,97,98]

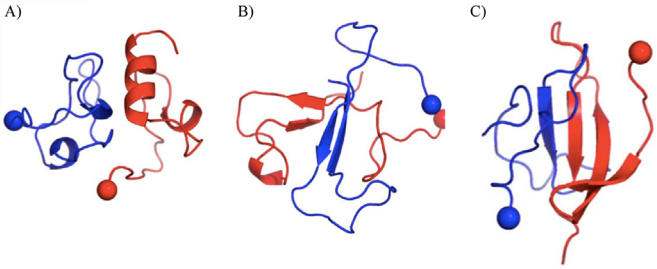

Figure 5. Representative structures of $A\beta_{1-40}$ dimer at 315 K for the WT, WT/A2V, A2V, and A2T peptides. The C_α atom of D1 is represented by a sphere. A) All-alpha topologies; B) all-beta topologies with two double β-hairpins; and C) an intramolecular 3-stranded β-sheet.

5 FAD Mutations on the Dimer Structure of $A\beta_{1-40}/A\beta_{1-42}$ Peptides

Familial forms of Alzheimer's disease (FAD) represent only a small fraction of all AD cases. Here, we only discuss the mutations located within residues 672–714 of APP, from which $A\beta_{42}$ is processed. Although the addition of the residues IA at positions 41 and 42 increases the pathogenic character of the Aβ peptide and a high percentage of Aβ with a Met-sulfoxide at position 35 is present in the AD brain, the C-terminus is devoid of FAD mutations.[1]

The most common mutations located in the loop and near CHC, the Flemish (A21G), Dutch (E22Q), Italian (E22K), Arctic (E22G), and Iowa (D23N) mutations, and in the N-terminus, FAD H6R (English), D7H (Taiwanese), and D7N (Tottori), are known to increase Aβ propensity to aggregate *in vitro* and the toxicity mediated by Aβ.[1] Using IM-MS experiments, Gessel *et al.* showed that the D7N, A21G, and E22G peptides display very different oligomer distributions with respect to the WT results, that also vary from $A\beta_{1-40}$ to $A\beta_{1-42}$.[99] Two other FAD mutations exist near the CHC: the Osaka E22Δ mutation consisting of a deletion of residue 22, and K16N, which is itself not harmful, but becomes toxic when mixed upon an equimolar ratio of WT.[1,100]

Using Markov state models and the potential of mean force calculations, Xu *et al.* showed that one FAD mutation changes the rugged free-energy landscapes of the $A\beta_{1-42}$ monomer by altering the energy barriers around basins. The E22 (E22Δ, E22G, E22K, and E22Q) and D23N mutants generate more hub-like microstates than $A\beta_{42}$ WT, offering, therefore, alternative pathways for transitions that could explain enhanced aggregation kinetics.[101] Based on the thousands of all-atom MD simulations of the $A\beta_{1-42}$ monomer in explicit solvent, a link between α-helix propensity and aggregation kinetics was proposed by Lin *et al.*[102] Based on REMD simulations with various force fields, Garcia *et al.* showed that these mutations increase interactivity of the N-terminus in β pairing that could allow for the seeding of different oligomers and faster aggregation pathways.[94]

Insights into the impact of FAD mutations on $A\beta_{1-40}$ and $A\beta_{1-42}$ dimers were investigated using different simulation conditions and extent of sampling. Atomistic MD simulations reported a decrease in β-strand propensity, an increase of the flexibility of CHC, and a change in contact maps in $A\beta_{1-40}$ and $A\beta_{1-42}$ dimers upon A21G substitution.[103] CG DMD simulations with implicit solvent showed the destabilizing effect of E22G mutation on the structure of residues 20–30 and its increased β-strand impact on the N-terminus of dimers.[31] The other mutations at the position 22 were also found to impact the CHC and the global topologies.[31] OPEP CG REMD simulations of $A\beta_{1-40/1-42}$ dimers in implicit solvent showed that the $A\beta_{1-40}$ D23N dimer exhibits structural motifs that differ from those observed in $A\beta_{1-40}$ WT and $A\beta_{1-42}$ WT. For instance, while its C-terminal has a higher β-strand propensity than in $A\beta_{1-40}$, its CHC is almost free from secondary structure, as opposed to $A\beta_{1-42}$.[81]

All-atom MD simulations of the $A\beta_{1-40/1-42}$ dimers in explicit solvent proposed different mechanisms for the increased Aβ aggregation upon FAD D7N and H6R mutations. The D7N mutation could accelerate the kinetics by reducing the bending free energy of the loop region;[104] while, upon H6R mutation, the aggregation kinetics of $A\beta_{1-42}$ could increase due to an enhanced β-strand at the C-terminus and higher stability of the salt bridge D23-K28.[105]

While these simulations help understand the increase in aggregation kinetics upon mutations, the structural characterization of FAD dimers remains, in our opinion, very elusive. What is clear from experiments and simulations is that the results obtained on $A\beta_{1-40}$ cannot be transposed to $A\beta_{1-42}$, but whether the variations observed between the mutants arise from differences in simulation details or analysis has to be explored.

6 Protective Mutations on $A\beta_{1-40}/A\beta_{1-42}$ Dimer Structures

While the FAD and A2V mutations increase aggregation Aβ kinetics, the A2T mutation and the equimolar mixture of the WT and A2V peptides (WT/A2V), and of the WT and A2T peptides (WT/A2T), retard kinetics.[106–110] Heterozygous carriers of A2V, and both homozygous and heterozygous carriers of A2T are protected against AD.[106,111] A2T reduces the production of Aβ from APP by 20–40 %, in contrast to A2V, which enhances Aβ production.[106,111] *In vitro* experiments have shown that A2V, WT/A2V, and WT/A2T change the oligomer size distributions and the stability of the oligomers.[106–110] For instance, by using IM-MS, A2V caused $A\beta_{1-40}$ to aggregate similarly to $A\beta_{1-42}$ WT with the formation of dimers, tetramers, hexamers, and dodecamers, while the WT/A2V mixture inhibited formation of hexamers and dodecamers.[112] Unique morphologies of the A2T aggregates were also observed using atomic force microscopy.[110]

As a first step towards determining the impact of the single A2V mutation, Nguyen *et al.* found, by atomistic REMD simulations, that the $A\beta_{1-28}$ A2V monomer is much less intrinsically disordered than the WT peptide, has a higher propensity to form β-hairpins, and displays a conformational ensemble totally different from that observed in WT.[113] The monomer structures of $A\beta_{1-40/1-42}$ A2T were also investigated by two REMD simulations differing in force field and simulation time: 175 ns/replica[113] vs. 500–1000 ns/replica.[94] It was shown that this mutation encourages the N-terminus to engage distant regions of the peptide and increases the N-terminus in

β pairing, leading to the possibility of more diverse β topologies.

Next, we compared the equilibrium structures of the $A\beta_{1-40}$ A2V and A2V/WT dimers with the structures of the WT dimer using extensive atomistic REMD simulations at pH 7 with 400 ns per replica. As $A\beta_{1-40}$ peptide is much less prone to aggregation than the more toxic $A\beta_{1-42}$ peptide, our predictions can be more easily tested experimentally. Our simulations reveal that, while the mean secondary structure composition is almost unchanged, there are drastic differences in the intramolecular conformations, and tertiary and quaternary structures upon single and double A2V mutation.[115]

The intrinsic disorder and the intermolecular potential energies are reduced upon A2V mutation with respect to WT. In contrast, the A2V and WT have similar intrinsic disorder and the A2V dimer states have more favourable interpeptide energies than the WT states. The WT and A2V peptides display many all-α topologies (Figure 5A), whereas WT/A2V is almost devoid of them. Very interestingly, the population of the intramolecular 3-stranded β-sheet spanning Nter-CHC-Cter (Figure 5C) ranks in the order: WT/A2V (23%) > WT (15%) and A2V (9%), correlating with the increase in the experimental lag phases. The presence of this transient N-terminal β-strand in $A\beta_{1-40}$ dimers upon single A2V mutation is likely to increase the free-energy barrier to convert one molecule to its aggregation-prone state.[115]

Whether the protective effect of A2T in the heterozygous form can be rationalized similarly on the $A\beta_{1-40}$ dimer was recently examined by atomistic REMD simulations.[116] We find that the calculated binding free energies correlate well with the observed kinetics of fibril formation, and the intramolecular 3-stranded β-sheet is an appropriate variable to differentiate fast (A2V, WT) from slow (WT/A2V, WT/A2T) aggregation-prone sequences. The corresponding values are 9% in A2V and 15% in WT vs. 23% in WT/A2V and 25% in WT/A2T.[116] It would be interesting to study the $A\beta_{1-40}$ A2T dimer to determine whether we can propose a theoretical framework that unifies the experimental results on the assembly kinetics of the protective mutations in heterozygous and homozygous cases.

7 Conclusion

We have reviewed what our computer simulations based on off-lattice and on-lattice protein models can tell us about Aβ self-assembly and its link to Alzheimer's disease. For each of the five aspects considered, we have looked at dynamic and thermodynamic properties in aqueous solution. It is clear that these simulations should be repeated including metal ions, main protein receptors, and the membrane, so as to be closer to *in cell* conditions.

Acknowledgements

We acknowledge support from the GRAL ANR SIMI 12-BS07-0017-01, Pierre Gilles de Gennes Foundation, "DYNAMO" ANR-11-LABX-0011, IDRIS computer time (grant x2015077198), and the European Research Council (FP7/2007-2013, Grant Agreement no. 258748).

References

[1] J. Nasica-Labouze, P. H. Nguyen, F. Sterpone, O. Berthoumieu, N. V. Buchete, S. Coté, A. De Simone, A. J. Doig, P. Faller, A. Garcia, A. Laio, S. L. Mai, S. Melchionna, N. Mousseau, Y. Mu, A. Paravastu, S. Pasquali, D. J. Rosenman, B. Strodel, B. Tarus, J. H. Viles, T. Zhang, C. Wang, P. Derreumaux, *Chem. Rev.* **2015**, *115*, 3518–3563.

[2] D. J. Selkoe, J. Hardy, *EMBO Mol. Med.* **2016**, doi: 10.15252/emmm.201606210.

[3] J. M. Nussbaum, S. Schilling, H. Cynis, A. Silva, E. Swanson, T. Wangsanut, K. Tayler, B. Wiltgen, A. Hatami, R. Rönicke, K. Reymann, B. Hutter-Paier, A. Alexandru, W. Jagla, S. Graubner, C. G. Glabe, H.-U. Demuth, G. S. Bloom, *Nature* **2012**, *485*, 651–655.

[4] A. Lacour, A. Espinosa, E. Louwersheimer, S. Heilmann, I. Hernández, S. Wolfsgruber, V. Fernández, H. Wagner, M. Rosende-Roca, A. Mauleón, S. Moreno-Grau, L. Vargas, Y. A. Pijnenburg, T. Koene, O. Rodríguez-Gómez, G. Ortega, S. Ruiz, H. Holstege, O. Sotolongo-Grau, J. Kornhuber, O. Peters, L. Frölich, M. Hüll, E. Rüther, J. Wiltfang, M. Scherer, S. Riedel-Heller, M. Alegret, M. M. Nöthen, P. Scheltens, M. Wagner, L. Tárraga, F. Jessen, M. Boada, W. Maier, W. M. van der Flier, T. Becker, A. Ramirez, A. Ruiz, *Mol. Psychiatry* **2016**, doi: 10.1038/mp.2016.18.

[5] M. Matarin, D. A. Salih, M. Yasvoina, D. M. Cummings, S. Guelfi, W. Liu, M. A. Nahaboo Solim, T. G. Moens, R. M. Paublete, S. S. Ali, M. Perona, R. Desai, K. J. Smith, J. Latcham, M. Fulleylove, J. C. Richardson, J. Hardy, F. A. Edwards, *Cell Rep.* **2015**, *10*, 633–644.

[6] A. J. Doig, P. Derreumaux, *Curr. Opin. Struct. Biol.* **2015**, *30*, 50–56.

[7] D. J. Rosenman, C. R. Connors, W. Chen, C. Wang, A. E. Garcia, *J. Mol. Biol.* **2013**, *425*, 3338–3359.

[8] A. Müller-Schiffmann, A. Herring, L. Abdel-Hafiz, A. N. Chepkova, S. Schäble, D. Wedel, A. H. Horn, H. Sticht, M. A. de Souza Silva, K. Gottmann, O. A. Sergeeva, J. P. Huston, K. Keyvani, C. Korth, *Brain* **2016**, *39*, 509–525.

[9] A. Müller-Schiffmann, A. Andreyeva, A. H. Horn, K. Gottmann, C. Korth, H. Sticht, *ACS Chem. Neurosci.* **2011**, *2*, 242–248.

[10] A. Waudby, G. L. Devlin, S. I. Cohen, A. Aguzzi, M. Vendruscolo, E. M. Terentjev, M. E. Welland, C. M. Dobson, *Science* **2009**, *326*, 1533–1537.

[11] A. Šarić, Y. C. Chebaro, T. P. Knowles, D. Frenkel, *Proc. Natl. Acad. Sci. U. S. A.* **2014**, *111*, 17869–17874.

[12] M. So, D. Hall, Y. Goto, *Curr. Opin. Struct. Biol.* **2016**, *36*, 32–39.

[13] P. Ghosh, A. Vaidya, A. Kumar, V. Rangachari, *Math. Biosci.* **2016**, *273*, 70–79.

[14] Y. Chebaro, P. Derreumaux, *Proteins Struct. Funct. Bioinf.* **2009**, *75*, 442–452.

[15] Y. Chebaro, P. Jiang, T. Zhang, Y. Mu, P. H. Nguyen, N. Mousseau, P. Derreumaux, *J. Phys. Chem. B* **2012**, *116*, 8412–8422.
[16] T. Zhang, J. Zhang, P. Derreumaux, Y. Mu, *J. Phys. Chem. B* **2013**, *117*, 3993–4002.
[17] T. Zhang, W. Xu, Y. Mu, P. Derreumaux, *ACS Chem. Neurosci.* **2014**, *5*, 148–159.
[18] B. Tarus, P. H. Nguyen, O. Berthoumieu, P. Faller, A. J. Doig, P. Derreumaux, *Eur. J. Med. Chem.* **2015**, *91*, 43–50.
[19] O. Berthoumieu, P. H. Nguyen, M. P. Castillo-Frias, S. Ferre, B. Tarus, J. Nasica-Labouze, S. Noël, O. Saurel, C. Rampon, A. J. Doig, P. Derreumaux, P. Faller, *Chemistry* **2015**, *21*, 12657–12666.
[20] H. Li, Y. Luo, P. Derreumaux, G. Wei, *Biophys. J.* **2011**, *101*, 2267–2276.
[21] Z. Fu, Y. Luo, P. Derreumaux, G. Wei, *Biophys. J.* **2009**, *97*, 1795–1803.
[22] M. H. Viet, P. Derreumaux, M. S. Li, C. Roland, C. Sagui, P. H. Nguyen, *J. Chem. Phys.* **2015**, *143*, 155101.
[23] a) P. Derreumaux, *J. Chem. Phys.* **1997**, *107*, 1941–1947; b) P. Derreumaux, *J. Chem. Phys.* **1997**, *106*, 5260–5270.
[24] P. Derreumaux, *J. Chem. Phys.* **1999**, *111*, 2301–2310.
[25] S. J. Marrink, D. P. Tieleman, *Chem. Soc. Rev.* **2013**, *42*, 6801–6822.
[26] R. Pellarin, P. Schuetz, E. Guarnera, A. Caflisch, *J. Am. Chem. Soc.* **2010**, *132*, 14960–14970.
[27] G. Bellesia, J. E. Shea, *J. Chem. Phys.* **2009**, *130*, 145103.
[28] F. Sterpone, P. H. Nguyen, M. Kalimeri, P. Derreumaux, *J. Chem. Theory. Comput.* **2013**, *9*, 4574–4584.
[29] F. Sterpone, S. Melchionna, P. Tuffery, S. Pasquali, N. Mousseau, T. Cragnolini, Y. Chebaro, J.-F. St-Pierre, M. Kalimeri, A. Barducci, Y. Laurin, A. Tek, M. Baaden, P. H. Nguyen, P. Derreumaux, *Chem. Soc. Rev.* **2014**, *43*, 4871–4893.
[30] M. Cheon, I. Chang, C. K. Hall, *Proteins Struct. Funct. Bioinf.* **2010**, *78*, 2950–2960.
[31] B. Urbanc, M. Betnel, L. Cruz, G. Bitan, D. B. Teplow, *J. Am. Chem. Soc.* **2010**, *132*, 4266–4280.
[32] P. Derreumaux, *Phys. Rev. Lett.* **2000**, *85*, 206–209.■■not called in text■■
[33] G. Wei, N. Mousseau, P. Derreumaux, *J. Chem. Phys.* **2003**, *119*, 6403–6409.
[34] A. Barducci, M. Bonomi, P. Derreumaux, *J. Chem. Theory. Comput.* **2011**, *7*, 1928–1934.
[35] Y. Chebaro, S. Pasquali, P. Derreumaux, *J. Phys. Chem. B* **2012**, *116*, 8741–8752.
[36] a) Y. Shen, J. Maupetit, P. Derreumaux, P. Tufféry, *J. Chem. Theory. Comput.* **2014**, *10*, 4745–4758; b) P. Thévenet, Y. Shen, J. Maupetit, F. Guyon, P. Derreumaux, P. Tufféry, *Nucleic Acids Res.* **2012** (Web Server issue), W288–293; c) J. Maupetit, P. Derreumaux, P. Tuffery, *Nucleic Acids Res.* **2009** (Web Server issue), W498–503.
[37] M. Kalimeri, P. Derreumaux, F. Sterpone, *J. Non-Cryst. Solids* **2015**, *407*, 494–501.
[38] P. Kynast, P. Derreumaux, B. Strodel, *BMC Biophys.* **2016**, *9*, 4.
[39] D. Matthes, V. Gapsys, B. L. de Groot, *J. Mol. Biol.* **2012**, *421*, 390–416.
[40] D. W. Li, S. Mohanty, A. Irback, S. Huo, *PLoS Comput. Biol.* **2008**, *4*, e1000238.
[41] J. Nasica-Labouze, M. Meli, P. Derreumaux, G. Colombo, N. Mousseau, *PLoS Comput. Biol.* **2011**, *7*, e1002051.
[42] A. Morriss-Andrews, J. E. Shea, *J. Phys. Chem. Lett.* **2014**, *5*, 1899–1908.
[43] M. Carballo-Pacheco, B. Strodel, *J. Phys. Chem. B* **2016**, *120*, 2991–2999.
[44] a) G. Wei, N. Mousseau, P. Derreumaux, *Biophys. J.* **2004**, *87*, 3648–3656; b) A. Melquiond, N. Mousseau, P. Derreumaux, *Proteins Struct. Funct. Bioinf.* **2006**, *65*, 180–191; c) G. Wei, N. Mousseau, P. Derreumaux, *Prion* **2007**, *1*, 3–8.
[45] C. Liu, M. R. Sawaya, P. N. Cheng, J. Zheng, J. S. Nowick, D. Eisenberg, *J. Am. Chem. Soc.* **2011**, *133*, 6736–6744.
[46] W. Song, G. Wei, N. Mousseau, P. Derreumaux, *J. Phys. Chem. B* **2008**, *112*, 4410–4418.
[47] A. Laganowsky, C. Liu, M. R. Sawaya, J. P. Whitelegge, J. Park, M. Zhao, A. Pensalfini, A. B. Soriaga, M. Landau, P. K. Teng, D. Cascio, C. Glabe, D. Eisenberg, *Science* **2012**, *335*, 1228–1231.
[48] A. De Simone, P. Derreumaux, *J. Chem. Phys.* **2010**, *132*, 165103.
[49] T. D. Do, N. E. Lapointe, R. Nelson, P. Krotee, E. Y. Hayden, B. Ulrich, S. Quan, S. C. Feinstein, D. B. Teplow, D. Eisenberg, J. E. Shea, M. T. Bowers, *J. Am. Chem. Soc.* **2016**, *138*, 549–557.
[50] S. Santini, G. Wei, N. Mousseau, P. Derreumaux, *Structure* **2004**, *12*, 1245–1255.
[51] S. Santini, N. Mousseau, P. Derreumaux, *J. Am. Chem. Soc.* **2004**, *126*, 11509–11516.
[52] S. A. Petty, S. M. Decatur, *Proc. Natl. Acad. Sci. U. S. A.* **2005**, *102*, 14272–14277.
[53] M. Kittner, V. Knecht, *J. Phys. Chem. B* **2010**, *114*, 15288–15295.
[54] B. Strodel, C. S. Whittleston, D. J. Wales, *J. Am. Chem. Soc.* **2007**, *129*, 16005–16014.
[55] Y. Lu, P. Derreumaux, Z. Guo, N. Mousseau, G. Wei, *Proteins Struct. Funct. Bioinf.* **2009**, *75*, 954–963.
[56] F. Baftizadeh, F. Pietrucci, X. Biarnes, A. Laio, *Phys. Rev. Lett.* **2013**, *110*, 168103.
[57] P. H. Nguyen, P. Derreumaux, *J. Phys. Chem. B* **2013**, *117*, 5831–5840.
[58] J. P. Colletier, A. Laganowsky, M. Landau, M. Zhao, A. B. Soriaga, L. Goldschmidt, D. Flot, D. Cascio, M. R. Sawaya, D. Eisenberg, *Proc. Natl. Acad. Sci. U. S. A.* **2011**, *108*, 16938–16943.
[59] E. L. Ermak, J. A. McCammon, *J. Chem. Phys.* **1978**, *69*, 1352–1360.
[60] M. Bernaschi, S. Melchionna, S. Succi, M. Fyta, E. Kaxiras, J. K. Sircar, *Comput. Phys. Commun.* **2009**, *180*, 1495–1502.
[61] T. Frembgen-Kesner, A. H. Elcock, *J. Chem. Theory. Comput.* **2009**, *5*, 242–256.
[62] F. Sterpone, P. Derreumaux, S. Melchionna, *J. Chem. Theory. Comput.* **2015**, *11*, 1843–1853.
[63] G. Meisl, X. Yang, B. Frohm, T. P. Knowles, S. Linse, *Sci. Rep.* **2016**, *6*, 18728.
[64] K. Garai, B. Sahoo, P. Sengupta, S. Maiti, *J. Chem. Phys.* **2008**, *128*, 045102.
[65] S. I. Cohen, S. Linse, L. M. Luheshi, E. Hellstrand, D. A. White, L. Rajah, D. E. Otzen, M. Vendruscolo, C. M. Dobson, T. P. Knowles, *Proc. Natl. Acad. Sci. U. S. A.* **2013**, *110*, 9758–9763.
[66] R. Cabriolu, S. Auer, *J. Mol. Biol.* **2011**, *411*, 275–285.
[67] J. Zhang, M. Muthukumar, *J. Chem. Phys.* **2009**, *130*, 035102.
[68] M. S. Li, N. T. Co, G. Reddy, C. K. Hu, J. E. Straub, D. Thirumalai, *Phys. Rev. Lett.* **2010**, *105*, 218101.

[69] J. A. Luiken, P. G. Bolhuis, *J. Phys. Chem. B* **2015**, *119*, 12568–12579.
[70] U. F. Rohrig, A. Laio, N. Tantalo, M. Parrinello, R. Petrozio, *Biophys. J.* **2006**, *91*, 3217–3229.
[71] R. D. Hills, C. L. Brooks III, *J. Mol. Biol.* **2007**, *368*, 894–901.
[72] Y. Zou, Y. Sun, Y. Zhu, B. Ma, R. Nussinov, Q. Zhang, *ACS Chem. Neurosci.* **2016**, *7*, 286–296.
[73] P. Nguyen, M. S. Li, J. E. Straub, D. Thirumalai, *Proc. Natl. Acad. Sci. U. S. A.* **2007**, *104*, 111–116.
[74] F. Baftizadeh, X. Biarnes, F. Pietrucci, F. Affinito, A. Laio, *J. Am. Chem. Soc.* **2012**, *134*, 3886–3694.
[75] N. T. Co, M. S. Li, *J. Chem. Phys.* **2012**, *137*, 095101.
[76] A. Irback, S. E. Jonsson, N. Linnemann, B. Linse, S. Wallin, *Phys. Rev. Lett.* **2013**, *110*, 058101.
[77] S. Abeln, M. Vendruscolo, C. M. Dobson, D. Frenkel, *PLoS One* **2014**, *9*, e85185.
[78] T. T. Tran, P. H. Nguyen, P. Derreumaux, *J. Chem. Phys.* **2016**, *144*, 205103.
[79] R. Nelson, M. R. Sawaya, M. Balbirnie, A. Madsen, C. Riekel, R. Grothe, D. Eisenberg, *Nature* **2005**, *435*, 773–778.
[80] R. Tycko, R. B. Wickner, *Acc. Chem. Res.* **2013**, *46*, 1487–1496.
[81] S. Côté, R. Laghaei, P. Derreumaux, N. Mousseau, *J. Phys. Chem. B* **2012**, *116*, 4043–4055.
[82] B. Barz, B. Urbanc, *PloS One* **2012**, *7*, e34345.
[83] B. Tarus, T. T. Tran, J. Nasica-Labouze, F. Sterpone, P. H. Nguyen, P. Derreumaux, *J. Phys. Chem. B* **2015**, *119*, 10478–10487.
[84] K. Lindorff-Larsen, S. Piana, R. O. Dror, D. E. Shaw, *Science* **2011**, *334*, 517–520.
[85] T. Zhang, P. H. Nguyen, J. Nasica-Labouze, Y. Mu, P. Derreumaux, *J. Phys. Chem. B* **2015**, *119*, 6941–6951.
[86] S. L. Bernstein, N. F. Dupuis, N. D. Lazo, T. Wyttenbach, M. M. Condron, G. Bitan, D. B. Teplow, J. E. Shea, B. T. Ruotolo, C. V. Robinson, M. T. Bowers, *Nat. Chem.* **2009**, *1*, 326–331.
[87] M. Kłoniecki, A. Jabłonowska, J. Poznański, J. Langridge, C. Hughes, I. Campuzano, K. Giles, M. Dadlez, *J. Mol. Biol.* **2011**, *407*, 110–124.
[88] M. D. Kirkitadze, M. M. Condron, D. B. Teplow, *J. Mol. Biol.* **2001**, *312*, 1103–1119.
[89] K. Ono, M. M. Condron, D. B. Teplow, *Proc. Natl. Acad. Sci. U. S. A.* **2009**, *106*, 14745–14750.
[90] W. Song, Y. Wang, J. P. Colletier, H. Yang, Y. Xu, *Sci. Rep.* **2015**, *5*, 11024.
[91] D. Granata, F. Baftizadeh, J. Habchi, C. Galvagnion, A. De Simone, C. Camilloni, A. Laio, M. Vendruscolo, *Sci. Rep.* **2015**, *5*, 15449.
[92] S. Côté, P. Derreumaux, N. Mousseau, *J. Chem. Theory. Comput.* **2011**, *7*, 2584–2592.
[93] Y. Chebaro, N. Mousseau, P. Derreumaux, *J. Phys. Chem. B* **2009**, *113*, 7668–7675.
[94] D. J. Rosenman, C. Wang, A. E. García, *J. Phys. Chem. B* **2016**, *120*, 259–277.
[95] A. K. Das, A. Rawat, D. Bhowmik, R. Pandit, D. Huster, S. Maiti, *ACS Chem. Neurosci.* **2015**, *6*, 1290–1295.
[96] L. Nagel-Steger, M. C. Owen, B. Strodel, *ChemBioChem* **2016**, *17*, 657–76.
[97] A. K. Somavarapu, K. P. Kepp, *ChemPhysChem* **2015**, *16*, 3278–3289.
[98] P. H. Nguyen, M. S. Li, P. Derreumaux, *Phys. Chem. Chem. Phys.* **2011**, *13*, 9778–9788.
[99] M. M. Gessel, S. Bernstein, M. Kemper, D. B. Teplow, M. T. Bowers, *ACS Chem. Neurosci.* **2012**, *3*, 909–918.
[100] D. Kaden, A. Harmeier, C. Weise, L. M. Munter, V. Althoff, B. R. Rost, P. W. Hildebrand, D. Schmitz, M. Schaefer, R. Lurz, S. Skodda, R. Yamamoto, S. Arlt, U. Finckh, G. Multhaup, *EMBO Mol. Med.* **2012**, *4*, 647–659.
[101] L. Xu, S. Shan, X. Wang, *J. Phys. Chem. B* **2013**, *117*, 6206–6216.
[102] Y. S. Lin, V. S. Pande, *Biophys. J.* **2012**, *103*, L47–49.
[103] A. Huet, P. Derreumaux, *Biophys. J.* **2006**, *91*, 3829–3840.
[104] M. H. Viet, P. H. Nguyen, S. T. Ngo, M. S. Li, P. Derreumaux, P. *ACS Chem. Neurosci.* **2013**, *4*, 1446–1457.
[105] M. H. Viet, P. H. Nguyen, P. Derreumaux, M. S. Li, *ACS Chem. Neurosci.* **2014**, *5*, 646–657.
[106] G. Di Fede, M. Catania, M. Morbin, G. Rossi, S. Suardi, G. Mazzoleni, M. Merlin, A. R. Giovagnoli, S. Prioni, A. Erbetta, C. Falcone, M. Gobbi, L. Colombo, A. Bastone, M. Beeg, C. Manzoni, B. Francescucci, A. Spagnoli, L. Cantù, E. Del Favero, E. Levy, M. Salmona, F. Tagliavini, *Science* **2009**, *323*, 1473–1477.
[107] I. Benilova, R. Gallardo, A. A. Ungureanu, V. Castillo Cano, A. Snellinx, M. Ramakers, C. Bartic, F. Rousseau, J. Schymkowitz, B. De Strooper, *J. Biol. Chem.* **2014**, *289*, 30977–30989.
[108] J. A. Maloney, T. Bainbridge, A. Gustafson, S. Zhang, R. Kyauk, P. Steiner, M. van der Brug, Y. Liu, J. A. Ernst, R. J. Watts, J. K. Atwal, *J. Biol. Chem.* **2014**, *289*, 30990–31000.
[109] M. Messa, L. Colombo, E. del Favero, T. L. Cantù, T. Stoilova, A. Cagnotto, A. Rossi, M. Morbin, G. Di Fede, F. Tagliavini, M. Salmona, *J. Biol. Chem.* **2014**, *289*, 24143–24152.
[110] B. Murray, M. Sorci, J. Rosenthal, J. Lippens, D. Isaacson, P. Das, D. Fabris, S. Li, G. Belfort, *Proteins Struct. Funct. Bioinf.* **2016**, *84*, 488–500.
[111] T. Jonsson, J. K. Atwal, S. Steinberg, J. Snaedal, P. V. Jonsson, S. Bjornsson, H. Stefansson, P. Sulem, D. Gudbjartsson, J. Maloney, K. Hoyte, A. Gustafson, Y. Liu, Y. Lu, T. Bhangale, R. R. Graham, J. Huttenlocher, G. Bjornsdottir, O. A. Andreassen, E. G. Jönsson, A. Palotie, T. W. Behrens, O. T. Magnusson, A. Kong, U. Thorsteinsdottir, R. J. Watts, K. Stefansson, *Nature* **2012**, *488*, 96–99.
[112] X. Zheng, D. Liu, R. Roychaudhuri, D. B. Teplow, M. T. Bowers, *ACS Chem. Neurosci.* **2015**, *6*, 1732–1740.
[113] P. H. Nguyen, B. Tarus, P. Derreumaux, *J. Phys. Chem. B* 2014, 118, 501–510.
[114] P. Das, B. Murray, G. Belfort, *Biophys. J.* **2015**, *108*, 738–47.■■not called in text■■
[115] P. H. Nguyen, F. Sterpone, J. M. Campanera, J. Nasica-Labouze, P. Derreumaux, *ACS Chem. Neurosci.* **2016**, *7*, 823–32.
[116] P. H. Nguyen, R. Pouplana, F. Sterpone, P. Derreumaux, J. Campanera, **2016**, in preparation.

Received: May 28, 2016
Published online: ■■ ■■, 0000

Israel Journal of Chemistry

REVIEWS

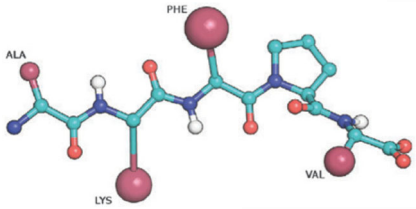

*M. Chiricotto, T. T. Tran, P. H. Nguyen, S. Melchionna, F. Sterpone, P. Derreumaux**

■■–■■

Coarse-grained and All-atom Simulations towards the Early and Late Steps of Amyloid Fibril Formation